Dalton Transactions

ROYAL SOCIETY OF CHEMISTRY

PAPER

View Article Online
View Journal | View Issue

Cite this: *Dalton Trans.*, 2026, **55**, 125

From speciation to action: Cu(II) and Zn(II) tune histatins, but pH and enamel drive efficacy

Emilia Dzień,[a] Aleksandra Mikołajczyk-Tarnawa,[b] Agnieszka Matera-Witkiewicz,*[b] Krzysztof Szewczyk,[c] Miquel Barceló-Oliver,[d] Lilla Pawlik-Sobecka,[e] Joanna Wątły[a] and Magdalena Rowińska-Żyrek*[a]

Histatins are histidine-rich salivary peptides whose antimicrobial activity emerges from a delicate interplay between proteolytic cleavage and metal coordination. We quantified Cu(II) and Zn(II) binding to histatin 1 and its hydrolytic products (histatin 1-2 and histatin 2), as well as to histatin 7 and histatin 9, and related thermodynamic and spectroscopic properties to *in vitro* activity. Histatins form stable metal complexes, with Cu(II) binding occurring primarily *via* the ATCUN motif in histatin 1 and histatin 1-2, and with Zn(II) coordination following the –HEXXH– motif. In contrast to simple electrostatic expectations, adding terminal Arg residues neither measurably stabilizes Zn(II) complexes nor enhances bactericidal activity. Across ATCC pathogens tested, activities remain modest and largely decoupled from complex stability, with only isolated effects upon metallation. Overall, two main conclusions may be drawn: (i) proteolysis mainly reshapes peptide topology and surface contacts rather than activating a metal-dependent mechanism and (ii) environmental pH together with anchoring to hydroxyapatite are likely the main drivers of efficacy *in situ*. We propose a working model in which site-selective hydrolysis positions histatins at the enamel–biofilm interface, while Cu(II)/Zn(II) binding acts as a structural governor rather than a direct antimicrobial switch. This reframes design rules for histatin-like therapeutics: optimize localization and pH-gated charge distribution first and then treat metallation as a context-dependent modulator.

Received 15th October 2025,
Accepted 18th November 2025

DOI: 10.1039/d5dt02485d

rsc.li/dalton

Introduction

Saliva is a key element of the innate immune system in humans and animals, as it contains antimicrobial peptides (AMPs). Among salivary AMPs, the following can be distinguished: lysozyme,[1] defensins (α- and β-defensins),[2] cystatins,[3] mucins,[4] statherin,[5] and histatins.[6] Histatins are a family of cationic, histidine-rich peptides varying in size between 7 and 38 amino acids.[6] The concentration of histatins in saliva extends from 17 to 33 μg mL^{-1},[7] of which about 80% are histatin 1, histatin 3 and histatin 5. Castagnola *et al.* observed that the highest concentration of histatins in saliva occurs around 5:00 and 6:00 p.m.[8] Johnson *et al.*, in turn, indicate a decrease in histatin concentration with age.[9] Histatins, as natural peptides, are sensitive to proteolytic cleavage; therefore, another factor influencing the concentration of histatins is the presence of proteolytic enzymes in saliva.[10,11] This is important due to differences in the antimicrobial activity of peptides from the histatin family. Of all histatins, histatin 5, which is one of the main proteolytic cleavage products of histatin 3,[12] demonstrates the greatest antifungal activity, especially against *Candida albicans*.[13] Recent work by Franz and co-workers has shown that well-defined Cu(II)-binding sites in histatin 5 can directly couple copper coordination to antifungal activity against *Candida albicans*.[14] The antimicrobial activity of histatins has also been demonstrated against ESKAPE pathogens.[15]

Histatins are mainly produced and released by the serous acini of the parotid, submandibular, sublingual and von Ebner glands.[16,17] Expression of histatin 1, as the only one of the histatin family, has also been found in human lacrimal glands, melanoma cell lines, metastatic lesions of melanoma patients[18,19] and head and neck squamous cell carcinoma (HNSCC) tumors.[20] The presence of histatin 1 in cancer tissues suggests the potential of using the peptide as a tumor marker.[19] Moreover, a recent study by Jenwanichkul *et al.* indicates the potential use of histatin 1 as an anticancer drug. Due to its cationic nature, it binds to the cancer cell membrane, leading to its disruption. Additionally, it has been noted that histatin 1 sensitizes cancer cells to the commonly used

[a]*Faculty of Chemistry, University of Wrocław, F. Joliot-Curie 14, 50-383 Wrocław, Poland. E-mail: magdalena.rowinska-zyrek@uwr.edu.pl*
[b]*Screening of Biological Activity Assays and Collection of Biological Material Laboratory, Faculty of Pharmacy, Wroclaw Medical University, Borowska 211A, 50-556 Wrocław, Poland. E-mail: agnieszka.matera-witkiewicz@umw.edu.pl*
[c]*Department of Oncology, Wrocław Medical University, pl. L. Hirszfelda 12, 53-413 Wrocław, Poland*
[d]*Department of Chemistry, University of Balearic Islands, Cra. de Valldemossa, km 7.5., 07122 Palma de Mallorca, Spain*
[e]*Department of Basic Medical Sciences, Faculty of Farmacy, Wroclaw Medical University, Borowska 211, Wroclaw, Poland*

drug cisplatin, which enhances its cytotoxicity.[21] In addition to its potential anticancer activity, histatin 1 also exhibits antifungal activity against *C. albicans* (strain B311 and ATCC 44505), although lower than that of histatin 3 and histatin 5.[22] In turn, in conjunction with statherin 1, it has an antibacterial effect by reducing the adhesion of the oral bacteria *Streptococcus mutans* to the hydroxyapatite surface,[23] which may limit the development of caries.[24,25] It is possible due to its full phosphorylation on serine 2, which allows histatin 1 to effectively bind to hydroxyapatite crystals,[26] influencing the acquisition of the enamel pellicle[27] and facilitating the remineralization of enamel lesions.[28] Moreover, as shown by McDonald *et al.*, the binding of histatin 1 to the hydroxyapatite surface protects it from the action of proteolytic enzymes.[29] In addition to its antimicrobial activity and role in maintaining tooth enamel homeostasis described above, histatin 1 promotes wound healing in the oral mucosa, skin and epithelial cells, *in vitro* and *in vivo*, by stimulating epithelial migration.[30–32]

Previously, we discussed the coordination chemistry and microbiological activity of histatin 3 and 5 and their hydrolysis products, *i.e.* histatin 3-4, histatin 4, histatin 5-8 and histatin 8 in complexes with Cu(II) and Zn(II) ions, showing that: (i) Cu(II) binds to the albumin-like binding motif, if available (in histatin 3-4, histatin 4, histatin 5-8 and histatin 8); (ii) Zn(II) most typically coordinates to either the carboxylate side chain of glutamic acid and two histidine imidazole groups or two histidyl residues, with polymorphic binding sites, where zinc is most likely bound to two different sets of $\{2N_{im}\}$, with two of such forms being in equilibrium; (iii) the antimicrobial efficacy of histatins and their complexes is highly pH-dependent, with Zn(II) coordination often enhancing their activity; and (iv) histatin 3-4 and histatin 5-8 undergo structural changes, adopting a more α-helical conformation after binding Zn(II).[33,34]

This study demonstrates the relationship between the coordination mode, thermodynamic properties and the antimicrobial effectiveness of (i) genetically encoded histatin 1[6,35] and products of its autoproteolysis: its N-terminal fragment (here called histatin 1-2) and histatin 2 and (ii) cleavage products of histatin 3 – histatin 7 and histatin 9 – in this case, the influence of non-binding arginine residues on the metal complex's thermodynamic stability is discussed (Fig. 1).

Experimental

Materials

All peptides, histatin 1 (DSHEKRHHGYRRKFHEKHHSHREFPFYGDYGSNYLYDN), the N-terminal fragment of histatin 1 (here called histatin 1-2, DSHEKRHHGYR), histatin 2 (RKFHEKHHSHREFPFYGDYGSNYLYDN), histatin 7 (RKFHEKHHSHRGY) and histatin 9 (RKFHEKHHSHRGYR) were purchased from KareBay Biochem (USA) (certified purity of 98%) and were used as received. The purity was checked potentiometrically. $Cu(ClO_4)_2{\cdot}6H_2O$ and $Zn(ClO_4)_2{\cdot}6H_2O$ were extra pure products (Sigma-Aldrich) and the concentrations of stock solutions of these salts were determined by inductively coupled plasma optical emission spectroscopy (ICP-OES). The carbonate-free stock solution of 0.1 M NaOH was purchased from Sigma-Aldrich and then potentiometrically standardized with the primary standard potassium hydrogen phthalate (KHP, 99.9% purity). The ionic strength (I) was adjusted to 0.1 M by addition of $NaClO_4$ (Sigma-Aldrich). Peptides were soluble in water solutions.

Name	Sequence
histatin 1	DSHEKRHHGYRRKFHEKHHSHREFPFYGDYGSNYLYDN
histatin 2	RKFHEKHHSHREFPFYGDYGSNYLYDN
N-terminal fragment of histatin 1 (histatin 1-2)	DSHEKRHHGYR
histatin 7	RKFHEKHHSHRGY
histatin 9	RKFHEKHHSHRGYR

Fig. 1 Amino acid sequence of histatin 1, histatin 1-2, histatin 2, histatin 7 and histatin 9. The Cu(II) binding ATCUN motif is underlined; Zn(II) binding –HEXXHH– and –HEXXH– motifs are marked in orange.

Mass spectrometric measurements

High-resolution mass spectra were obtained on a Shimadzu LCMS-9030 qTOF (Shimadzu, Kyoto, Japan) device, equipped with a standard ESI source and a Nexera X2 system, and a Bruker Apex Ultra FT-ICR mass spectrometer (Bruker Daltonik, Bremen, Germany), equipped with an Apollo II electrospray ionization source with an ion funnel. The Shimadzu LCMS-9030 qTOF was operated in positive and negative ion modes. The instrumental parameters were as follows: scan range: m/z 100–2000, nebulizing gas: nitrogen, nebulizing gas flow: 3.0 L·min^{-1}, drying gas flow: 10 L·min^{-1}, heating gas flow: 10 L·min^{-1}, interface temperature: 300 °C, desolvation line temperature: 400 °C, detector voltage: 2.02 kV, interface voltage: 4.0 kV, collision gas: argon, mobile phases: (A) H_2O + 0.1% HCOOH and (B) MeCN + 0.1% HCOOH, and mobile phase total flow: 0.3 mL min^{-1}. The Bruker Apex Ultra FT-ICR mass spectrometer was operated in positive ion mode. The instrumental parameters were as follows: scan range: m/z 100–2000, dry gas: nitrogen, temperature: 473 K, and ion energy: 5 eV. The capillary voltage was optimized to the highest S/N ratio, and it was 4200 V. The injection volume was optimized depending on the intensity of the signals observed in the mass spectrum within the range of 0.1 to 3 μL. The samples were prepared in a 1 : 1 methanol–water mixture at a pH value of 7.4. The sample concentration was $[ligand]_{tot}$ = 10^{-4} M and the M : L molar ratio was 1 : 1. The obtained data were processed using ACDLabs Spectrus Processor v2021.1.3 and Bruker Compass DataAnalysis 4.0 programs.

Potentiometric measurements

Proton–ligand and metal–ligand stability constants were calculated from titration curves carried out over the pH range of 2–11 at 298 K under an argon atmosphere and an ionic strength of 0.1 M ($NaClO_4$). The total volume of the solution used was 2.8 cm^3. The potentiometric titrations were performed using a Metrohm Titrando 905 titrator and a Mettler Toledo InLab Micro combination pH electrode. The thermostabilized glass cell was equipped with a magnetic stirring system and a microburette delivery tube. The solutions were titrated with 0.1 M carbonate-free NaOH. The electrodes were daily calibrated for hydrogen ion concentration by titrating 4 mM

$HClO_4$ with NaOH under the same experimental conditions as mentioned above. The purities and the exact concentrations of the ligand solutions were determined by the Gran method.[36] The ligand concentration was 0.5 mM and the ratio of Cu(II) and Zn(II) to the ligand was 0.8 : 1.

The standard potential and the slope of the electrode couple were computed by means of the GLEE program.[37] HYPERQUAD 2006 was used for the stability constant calculations.[38] The standard deviations were computed by HYPERQUAD 2006 and refer to random errors only. The constants for the hydrolytic Zn(II) species were used in these calculations.[39] The speciation and competition diagrams were computed with the HYSS program.[40]

Spectroscopic studies

The UV-Vis absorption spectra were recorded on a Jasco-730 spectrophotometer and circular dichroism (CD) measurements were obtained on a Chirascan VX spectropolarimeter at 25 °C. For both methods, spectra were collected over the 200–800 nm range using quartz cuvettes with 1 cm optical path length. To determine the secondary structure of the analyzed samples, measurements were made in the 180–250 nm range, using a quartz cuvette with an optical path of 0.01 cm. The concentrations of the solutions used for spectroscopic studies were similar to those employed in the potentiometric experiments. The metal : peptide ratio was 0.8 : 1. All spectroscopic measurements were recorded in the pH range of 3–11. The pH of the samples was adjusted with the appropriate amounts of $HClO_4$ and NaOH solutions. The UV-Vis and CD spectroscopy parameters were calculated from the spectra obtained at the pH values corresponding to the maximum concentration of each particular species, based on distribution diagrams. OriginPro 8 was used to process and visualize the obtained spectra.

Antimicrobial activity assay

Seven reference strains from ATCC (*Enterococcus faecalis* ATCC 29212, MRSA *Staphylococcus aureus* ATCC 43300, *Klebsiella pneumoniae* ATCC 700603, *Acinetobacter baumannii* ATCC 19606, *Pseudomonas aeruginosa* ATCC 27853, *Escherichia coli* ATCC 25922 and *Candida albicans* ATCC 10231) were used for antimicrobial activity assays. The MIC50, as the lowest concentration of the tested compound at which 50% growth of the isolates was inhibited, was determined by a microdilution method with spectrophotometric measurements according to ISO 20776-1:2019[41] and ISO 16256:2012,[42] whereas a modified Richard's method using the redox indicator (2,3,5-triphenyltetrazolium chloride, TTC) was used to determine the minimal bactericidal/fungicidal concentration (MBC/MFC).[43–45] Serial dilutions of the peptides in Tryptic Soy Broth (TSB), with or without an equimolar concentration of Cu(II) or Zn(II), were made on 96-well microplates in the range between 0.5 and 512 μg mL^{-1}. Tryptone Soya Agar (TSA) plates were inoculated with microbial strains from preformed stocks. After 24 h/37 °C incubation (for bacteria) or 24 h/25 °C (for fungi), a proper density of bacterial and fungal suspension was prepared using a densitometer (final inoculum 5×10^5 CFU mL^{-1}) in TSB. Positive (TSB + strain) and negative controls (only TSB) were also included in the test. Spectrophotometric solubility control of each peptide and the peptide–metal ion system was performed. To avoid using strains that had developed additional resistance, the following antibacterial/antifungal agents were used as positive controls, according to breakpoint values established by the EUCAST:[46,47] *E. faecalis*: 4 μg mL^{-1} levofloxacin, *S. aureus*: 1 μg mL^{-1} levofloxacin, *K. pneumoniae*: 4 μg mL^{-1} gentamicin, *A. baumannii*: 0.5 μg mL^{-1} levofloxacin, *P. aeruginosa*: 1 μg mL^{-1} levofloxacin, *E. coli*: 4 μg mL^{-1} gentamicin and *C. albicans*: 1 μg mL^{-1} amphotericin B. MIC was determined from a series of at least three experiments as the lowest concentration of an antimicrobial agent that decreased the measured microbial growth to 50% relative to the positive control.

Microplates were incubated at 37 ± 1 °C or 25 ± 1 °C for 24 h on a shaker (500 rpm). After this, the spectrophotometric measurement was performed at 580 nm and then 50 μL aliquots of 1% (m/v) 2,3,5-triphenyltetrazolium chloride (TTC) solution were added to each well. TTC is a commonly used indicator of cellular respiration. In oxidized form, TTC is colorless, while it turns pink after reduction due to reactions in the respiratory chain. MBC/MFC (Minimum Bactericidal/Fungicidal Concentration) can be defined as the lowest concentration required to kill a particular microbial strain, determined by visual analysis after 24 h incubation with TTC. The pink color indicates the presence of living microorganisms, while the lack of color indicates that the colonies do not survive. Thanks to both methods, MIC and MBC or MFC can be determined.

Neutral red (NR) uptake assay

The experiment was conducted according to the established protocol.[48] The cells were seeded into 96-well plates at a concentration of 1×10^4 cells per well. After reaching 80% confluency (usually after 24 h), the cells were treated with dedicated compounds with/without metal ions (concentrations to assess cytotoxicity for normal cells (L929)). Additionally, the following concentrations were used: 150, 100, 50, and 10 μM. Negative controls with medium only and positive controls with 1 μM staurosporine were also included. The cells were incubated for 24, 48 and 72 hours prior to the experiment. After the exposure, the medium was replaced with 40 μg mL^{-1} NR in the appropriate culture medium and the cells were further incubated for up to 3 hours. The cells were subsequently washed with phosphate-buffered saline (PBS) and the dye was extracted with NR destain solution (1% acetic acid, 50% ethanol, 49% deionized water). To form a homogeneous solution, plates with cells were shaken for 30 minutes before absorbance reading at 540 nm. Untreated cells (negative control) represented 100% potential cellular growth.

Results and discussion

To investigate the precise stoichiometry and structural and thermodynamic properties of the complexes of histatin 1, his-

tatin 1-2, histatin 2, histatin 7 and histatin 9 with Cu(II)/Zn(II) ions, a set of experimental methods were used: mass spectrometry (ESI-MS), potentiometric titrations, and UV-Vis and CD spectroscopy.

The mass spectra confirmed that the tested peptides, under the experimental conditions here employed, are capable of forming Cu(II) and Zn(II) complexes in a 1 : 1 (metal : ligand ratio) stoichiometry. Signals and isotopic distributions in the experimental and simulated spectra for the chosen signals are consistent and confirm the correct interpretation (Fig. S1A–J).

Protonation constants

Based on a series of potentiometric titrations, nineteen deprotonating constants (pK_a) were established for histatin 1, eight deprotonating constants (pK_a) for the N-terminal fragment of histatin 1 (histatin 1-2), thirteen deprotonating constants (pK_a) for histatin 2 and nine deprotonating constants (pK_a) for histatin 7 and histatin 9, respectively (Table S1). The determined values for the deprotonation of histidine residues (with pK_a values in the range of 5.32–8.00 for histatin 1, 5.76–7.33 for histatin 1-2, 5.64–7.28 for histatin 2, 5.56–7.26 for histatin 7 and 5.57–7.22 for histatin 9) are in agreement with those found in the literature for similar poly-His systems.[49–52]

Cu(II)complexes

Cu(II)-histatin 1. The Cu(II) coordination to histatin 1 starts at about pH 3.5 (Table S2 and Fig. S2A). In the first detected complex, $CuH_{13}L$, with a maximum at pH 4.5, the His3 imidazole, the N-terminal amine group and the two amides in between the two groups simultaneously bind Cu(II), resulting in a $\{N_{im}, NH_2, 2N^-\}$ binding mode. This is confirmed by the CD spectrum (Fig. S3B) through the bands appearing at 306 nm (amide nitrogen), 267 nm (N-terminal amine) and 252 nm (imidazole nitrogen). Also, the participation of four nitrogens in Cu(II) coordination is confirmed by the UV-Vis band at 532 nm (Fig. S3A) and the presence of two peaks typical of an albumin-like binding mode, with λ_{max} = 489 nm and λ_{min} = 576 nm at pH 4.5 in the CD spectra (Fig. S3B). UV-Vis (Fig. S3A) and CD (Fig. S3B) spectra do not change significantly in the pH range of 5.0–11.1 ($CuH_{11}L$, $CuH_{10}L$, CuH_8L, CuH_7L, CuH_6L, CuH_4L, CuH_2L, CuL and $CuH_{-2}L$), which means that the copper(II) coordination mode is the same for all calculated species.

Cu(II)-histatin 1-2. The first Cu(II) complex (CuH_3L) starts to form above pH 3.5 and reaches its maximum at pH 4.7 (Table S2 and Fig. S2B). The characteristic band in the UV-Vis spectrum at 526 nm (Fig. S4A) indicates that four nitrogen atoms are engaged in Cu(II) coordination. In turn, the presence of maximum bands in the CD spectrum (Fig. S4B) indicates which atoms are responsible for binding the metal ion – the band at 247 nm evidences the participation of the N-terminal amine group in coordination; the band at 271 nm is assigned to the imidazole ring and the band at 308 nm is attributed to the amide nitrogen in the coordination sphere. Additionally, the appearance of two characteristic CD bands with positive and negative Cotton effects at 491 nm and 570 nm suggests the formation of a square-planar complex. These data suggest a $\{N_{im}, NH_2, 2N^-\}$ donor set, with a specific albumin-like binding *via* the ATCUN motif. Above pH 5.0, the coordination mode for the next complex species (CuH_2L, CuHL, CuL, $CuH_{-1}L$ and $CuH_{-2}L$) remains unchanged. This is confirmed by the fact that there is no change in the position of most of the bands (only their intensity increases), both in the UV-Vis and CD spectra (Fig. S4A and B).

Cu(II)-histatin 2. Cu(II) coordination to histatin 2 starts above pH 4 (Table S2 and Fig. S2C). The first detected complex is CuH_8L, whose maximum occurs in the pH range of 5.0–7.0. The UV-Vis band at 550 nm (Fig. S5A), the charge-transfer band at 256 nm and the d–d transition band at 544 nm in the CD spectra (Fig. S5B) suggest the participation of three nitrogens in the Cu(II) coordination sphere, typically one from the histydyl imidazole ring and two from the amide groups. The side chains of two other histidines are most probably already deprotonated and do not take part in the coordination. Loss of the next proton leads to the formation of the CuH_7L form, with a pK_a of 8.08, and is related to the deprotonation of the third amide group bound to the central Cu(II) ion. The 4N coordination is confirmed by a significant shift in the UV-Vis spectra (from 550 nm to 521 nm, Fig. S5B) and the shift in the CD d–d transition band from 544 nm to 505 nm (Fig. S5B). Also, the appearance of the band at 627 nm in the CD spectra (Fig. S4C) is typical of the formation of a square-planar complex with a $\{N_{im}, 3N^-\}$ binding mode. The presence of further forms (CuH_5L, CuH_2L CuL, $CuH_{-2}L$ and $CuH_{-3}L$) arises from the deprotonation of non-binding amino acid residues (one His imidazole, one amino terminal group and four Tyr side chains) that do not affect the Cu(II) binding mode. The coordination of Cu(II) by one histidyl imidazole and up to three deprotonated amides generates a strongly polarized, locally charged environment in which the deprotonation of ε-NH_3^+ to neutral ε-NH_2 is electrostatically disfavoured, leading to an increase in the effective pK_a of lysine compared to the free ligand, which is the reason for the Lys side chain constants being outside the measuring scope of the electrode.

Histatin 2, just as histatin 4 (RKFHEKHHSHRGYRSNYLYDN), lacks the ATCUN motif. Its first 11 N-terminal amino acid residues are in the same sequence as histatin 4 (NH_2–RKFHEKHHSHR^{11}–). Based on the NMR spectrum of the Cu(II)-histatin 4 complex, which confirmed that the coordination $\{N_{im}, 3N^-\}$ mode involved His4 in the coordination sphere,[34] we may conclude that the coordination mode is analogous in this case.

Cu(II)-histatin 7. The first complex observed for histatin 7 is CuH_6L, with a maximum at pH 4.7 (Table S2 and Fig. S2D), most likely involving one His imidazole and one amide nitrogen in Cu(II) binding. The 2N coordination is confirmed by the d–d band in the UV-Vis spectrum at 655 nm (Fig. S6A). The loss of the next two protons leads to the CuH_5L and CuH_4L complex species, with pK_a values of 4.82 and 5.92, respectively, and is related to the deprotonation of two non-binding His residues. The next complex species, CuH_3L (pK_a = 6.82), dominates in solution at pH 7.2. At this pH, the shift and increase

in the intensity in the UV-Vis spectra (from 655 nm to 586 nm, Fig. S6A) suggest the participation of one more amide nitrogen atom in the metal coordination. The 3N coordination mode with a $\{N_{im}, 2N^-\}$ donor set is also confirmed by a charge-transfer band near 260 nm and a d–d transition band at 540 nm in the CD spectra (Fig. S6B). The subsequent complex form, CuH_2L, with a pK_a value of 7.61, is the most abundant at pH 8.3 and engages the third amide group in coordination. This binding mode is confirmed by a significant shift in the UV-Vis spectra (from 586 to 530 nm, Fig. S6A) and a shift in the CD d–d transition band from 540 nm to 502 nm (Fig. S6B). Also, the appearance of the band at 621 nm in the CD spectra (Fig. S6B) indicates the formation of a square-planar complex with a $\{N_{im}, 3N^-\}$ binding mode. Additionally, the participation of only one histidyl residue in the coordination was confirmed by NMR spectroscopy of the Cu(II)-histatin 4 complex (histatin 7 is a hydrolysis product of histatin 4 and similarly to histatin 4, it does not have the ATCUN motif).[34] The formation of the next species CuH, CuL, $CuH_{-1}L$, $CuH_{-2}L$ and $CuH_{-3}L$ with pK_a values of 8.96, 9.68, 10.19, 10.90 and 10.99, respectively, is most probably related to the deprotonation of the water molecule, the N-terminal amine group, one Tyr and two Lys side chains, which do not participate in metal coordination.

Stabilities and spectroscopic data for Cu(II)-histatin 9 are analogous to those of Cu(II)-histatin 7, which is discussed above as a representative example.

Zn(II) complexes

Zn(II)-histatin 1. Zinc starts coordinating to histatin 1 above pH 4. The first observed complex form, $ZnH_{13}L$, reaches its maximum at pH 5.0 (Fig. S8A) and most probably, the carboxylate side chain of glutamic acid and two histidine imidazoles bind Zn(II) ions. The next three forms, $ZnH_{12}L$, $ZnH_{11}L$ and $ZnH_{10}L$ (pK_a values of 5.26, 6.21 and 7.77, respectively) come from the deprotonation of non-coordinating His imidazoles. The ZnH_9L form, with a pK_a value of 8.88, probably arises from the deprotonation of a water molecule, which completes the coordination sphere. The Zn(II)-histatin 1 complex results in a $\{2N_{im}, O^-\}$ binding mode.

Zn(II)-histatin 1-2. The first detected species, with a maximum at pH 6.7 (Fig. S8B), is ZnH_3L and most likely, Zn(II) is already coordinated to the carboxylate side chain of Glu and two imidazole nitrogen atoms from the HEXXHH motif. The loss of the next proton leads to the formation of the ZnH_2L complex species, with a pK_a value of 7.25 and is, most likely, related to the deprotonation of a water molecule that completes the coordination sphere of the central Zn(II) atom. The next three deprotonations lead to the formation of the species ZnHL, ZnL and $ZnH_{-1}L$, with pK_a values of 8.44, 9.95 and 11.06, respectively, and likely refer to the deprotonation of the N-terminal amine group and tyrosine and lysine residues, which do not participate in the metal complexation.

Zn(II)-histatin 2. In the first detected complex, ZnH_8L, with its maximum concentration at pH 5.7 (Fig. S8C), the coordination of Zn(II) to the carboxylate side chain of Glu and two imidazole nitrogen atoms is suggested, resulting in a $\{2N_{im}, O^-\}$ binding mode. The next complex species, ZnH_7L, with a pK_a value of 6.97, is associated with the deprotonation of a non-binding His imidazole. The following complex species, ZnH_6L (pK_a = 8.82), is probably formed as a result of the deprotonation of a water molecule coordinated to the central Zn(II) ion. The coordination is in good agreement with our previous results,[33,34] due to the presence of the –HEXXH– motif in histatin's 2 sequence. The remaining two species, ZnH_4L and ZnH_3L, can be ascribed to the deprotonation of the N-terminal amine group and Tyr residue and do not affect the complex binding mode.

Zn(II)-histatin 7. The first complex for histatin 7, ZnH_5L, with a $\log\beta$ of 53.68, reaches its maximum at pH 6.1 (Fig. S8D) and most likely, the carboxylate side chain of Glu and two His imidazole nitrogens from the typical Zn(II)-binding motif, –HEXXH–, are involved in Zn(II) coordination. The next two forms, ZnH_4L and ZnH_3L, with pK_a values of 6.50 and 7.63, respectively, probably come from the deprotonation of two non-binding His imidazoles. Subsequently, the ZnH_2L (pK_a = 8.70) form is the most abundant at around pH 9.2. In this species, the deprotonation of a bound water molecule is observed. The last two forms, ZnHL and ZnL, with pK_a values of 9.78 and 10.54, respectively, arise from the deprotonation of the non-bonding N-terminal amine group and Tyr residue. The Zn(II)-histatin 7 complex results in a $\{2N_{im}, O^-\}$ binding mode.

In the case of the Zn(II)-histatin 9 complex, overall stabilities are very similar (Table S2 and Fig. S8E), so the coordination mode is analogous to the Zn(II)-histatin 7 one, with one extra deprotonation of a Lys residue (pK_a = 10.81).

Antimicrobial activity and cytotoxicity

Antimicrobial susceptibility testing was performed using an expanded panel of microorganisms: two Gram-positive (*E. faecalis* ATCC 29212 and MRSA *S. aureus* ATCC 43300), four Gram-negative (*K. pneumoniae* ATCC 700603, *A. baumannii* ATCC 19606, *P. aeruginosa* ATCC 27853, and *E. coli* ATCC 25922) and one fungal strain (*C. albicans* ATCC 10231). The results showed no MBC/MFC activity. MIC_{50} values were determined for all active compounds and their metal complexes (Table 1). Moreover, for all ligands, ligand–metal ion systems, and regular L929 cells, viability (NR assay) was over 90%. Thus it can be clearly assumed that the investigated histatin and histatin–metal ion connections are safe in the analysed concentration range.

The only two active compounds against the Gram-positive bacterium *S. aureus* were the complex of histatin 1 with Zn(II) ions (MIC = 256 μg mL^{-1}) and histatin 7 (MIC = 256 μg mL^{-1}). Native histatin 7 is also active against *E. faecalis* (MIC = 256 μg mL^{-1}). After binding both Cu(II) and Zn(II) ions, the biological effect against *E. faecalis* did not change compared to the native peptide (MIC = 256 μg mL^{-1}). Unlike the previously analysed histatins, at physiological pH, histatin 1 is moderately active against Gram-negative bacteria *P. aeruginosa* (MIC = 128 μg mL^{-1}) and *K. pneumoniae* (MIC = 128 μg mL^{-1}). In the case of *K. pneumoniae*, a microbiological effect is also observed for the

Table 1 *In vitro* antibacterial activity of histatin 1, histatin 1-2, histatin 2, histatin 7 and histatin 9 determined as a minimal inhibitory concentration (MIC) (μg mL^{-1}) at pH = 7.40; n/d, not determined. Experiments were performed for all compounds and their copper(II) and zinc(II) complexes according to the ISO 20776-1:2019[41] and ISO 16256:2012.[42] No MIC value was determined for *A. baumannii* ATCC 19606 and *E. coli* ATCC 25922. No MBC/MFC activity was observed after performing modified Richard's method.[43–45] Control experiments for metal ions can be found in ref. 49

Strain	*S. aureus* (+) ATCC 43300 MIC (μg mL^{-1})	*E. faecalis* (+) ATCC 29212 MIC (μg mL^{-1})	*P. aeruginosa* (−) ATCC 27853 MIC (μg mL^{-1})	*K. pneumoniae* (−) ATCC 700603 MIC (μg mL^{-1})	*C. albicans* ATCC 10231 MIC (μg mL^{-1})
Histatin 1	n/d	n/d	128	128	256
Cu(II)-histatin 1	n/d	n/d	n/d	128	256
Zn(II)-histatin 1	256	n/d	n/d	256	256
Histatin 1-2	n/d	n/d	n/d	n/d	256
Cu(II)-histatin 1-2	n/d	n/d	n/d	n/d	n/d
Zn(II)-histatin 1-2	n/d	n/d	n/d	n/d	256
Histatin 2	n/d	n/d	n/d	n/d	n/d
Cu(II)-histatin 2	n/d	n/d	n/d	n/d	256
Zn(II)-histatin 2	n/d	n/d	n/d	n/d	n/d
Histatin 7	256	256	n/d	n/d	n/d
Cu(II)-histatin 7	n/d	256	n/d	n/d	n/d
Zn(II)-histatin 7	n/d	256	n/d	n/d	n/d
histatin 9	n/d	n/d	n/d	n/d	n/d
Cu(II)-histatin 9	n/d	n/d	n/d	n/d	n/d
Zn(II)-histatin 9	n/d	n/d	n/d	n/d	n/d

copper(II) and zinc(II) complexes of histatin 1 (MIC = 128 μg mL^{-1} and 256 μg mL^{-1}, respectively), but the binding of the metal ion by this peptide does not enhance its antimicrobial properties.

Under the studied conditions, MICs for histatin 1 (128–256 μg mL^{-1}) exceed the typical whole-saliva histatin levels (with a median for histatin 1 ≈ 17 μg mL^{-1}; for total histatins ≈ 33 ± 17 μg mL^{-1});[7] however, local histatin 1 levels at the enamel–biofilm interface are expected to be considerably higher due to specific binding to hydroxyapatite and protection from proteolysis, which renders our activities compatible with a biologically relevant, interfacial mechanism of action rather than bulk-phase killing.

Histatin activity does not depend simply on Cu(II)/Zn(II) affinity or complex stoichiometry. Proteolytic trimming changes peptide topology and redistributes positive charge, which modulates binding to hydroxyapatite and the pellicle and the electrostatic interaction with bacterial surfaces. Coordination of Cu(II) at the ATCUN site and of Zn(II) at the –HEXXH– motif mainly restricts backbone flexibility and does not uniformly increase activity; the secondary structure remains largely unchanged after metal binding and MIC values do not consistently decrease. *In vivo*, three factors appear critical: (i) localization at the enamel or pellicle, which concentrates the peptide and limits proteolysis; (ii) pH-dependent protonation, which enhances surface attraction; and (iii) metal availability, which is lowered by competing salivary ligands. Within this framework, metal coordination fine-tunes conformation and speciation but is not the principal determinant of the antimicrobial effect. This is consistent with the lack of benefit from adding terminal arginine residues and with the higher activity of native histatin 7 over its Arg-extended variant against selected Gram-positive strains.

A comparison of metal binding abilities

Histatins form thermodynamically stable complexes with Cu(II) and Zn(II) (Table S2). As expected, histatin 1 and its N-terminal fragment (histatin 1-2), in which the ATCUN motif is present, bind Cu(II) more effectively compared to histatins 2, 7 and 9, in which the copper ions are coordinated by the histidine imidazole and three amide nitrogens (Fig. 2A). Histatin 1 is a more effective Cu(II) binder, most likely because of the longer C-terminal part (as compared to histatin 2), which is able to sterically protect the metal binding site by (i) partial wrapping of the ATCUN site, (ii) providing additional electrostatic and hydrogen-bonding interactions, and (iii) favouring a conformation that shields the Cu(II) site from solvent.

Across the Zn(II) series, coordination involves two His imidazoles and a Glu carboxylate within the –HEXXH motif; sequence context matters, yet the longest peptides do not uniformly outperform shorter ones – histatins 1 and 2 show the greatest affinity towards Zn(II) in almost the entire tested pH range. This is probably related to the presence of the –FPF– sequence near the metal ion binding site. Proline, due to its unique cyclic structure that restricts rotation around the peptide bond, limits the flexibility of the peptide, resulting in local rigidity of the peptide chain.[53] In turn, the proximity of two phenylalanine residues may influence the formation of hydrophobic interactions or π–π stacking interactions, stabilizing the local structure of the peptide.[54] It is worth noting that the HEKHH motif, present in histatins 1 and 2, is a much more tempting site for Zn(II) than the HEKRHH site available in histatin 1-2. This finding highlights the importance of the non-binding residues in the typical –HEXXH– Zn(II) binding motif.

Due to the similarity of the amino acid sequence of histatin 7, histatin 8 and histatin 9, it was intriguing to compare the stability of the complexes of these peptides with Cu(II) and Zn(II). The case of Cu(II) complexes is what may have been expected – the Cu(II)-histatin 8 complex, in which the metal ion is coordinated by the N-terminus, the imidazole nitrogen of histidine in position 3 and two amide nitrogens in between

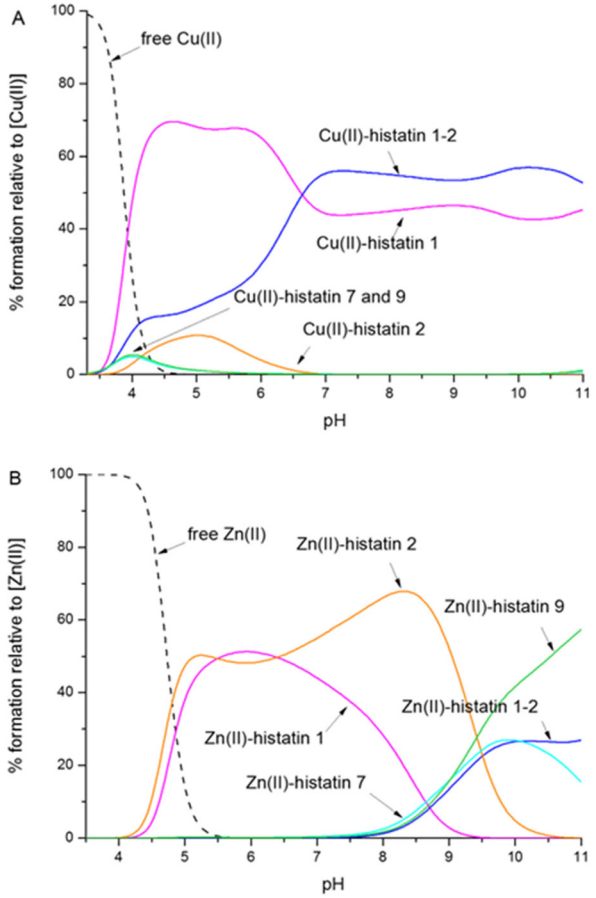

Fig. 2 Competition plots between histatin 1, histatin 1-2, histatin 2, histatin 7 and histatin 9 binding (A) Cu(II) and (B) Zn(II). The plots describe the complex formation at different pH values in a hypothetical situation, in which equimolar amounts of reagents are mixed. Calculations are based on binding constants from Table S2. Conditions: T = 298 K, [Cu(II)/Zn(II)] = [histatin 1] = [histatin 1-2] = [histatin 2] = [histatin 7] = [histatin 9] = 0.001 M.

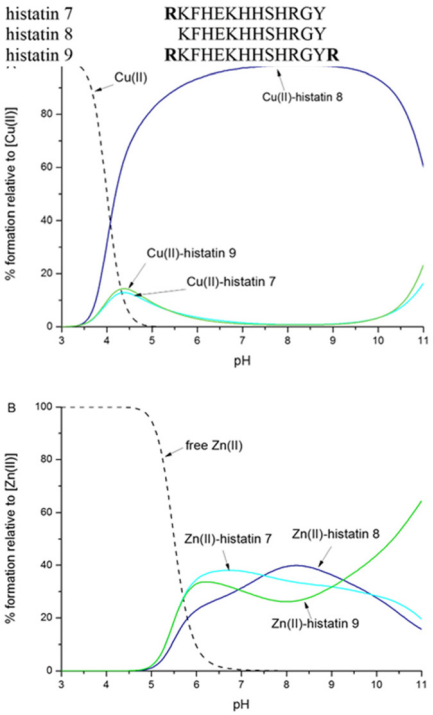

Fig. 3 Competition plots between histatin 7, histatin 8 and histatin 9 binding (A) Cu(II) and (B) Zn(II). The plots describe the complex formation at different pH values in a hypothetical situation, in which equimolar amounts of reagents are mixed. Calculations are based on binding constants from Table S2 and ref. 33. Conditions: T = 298 K, [Cu(II)/Zn(II)] = [histatin 7] = [histatin 8] = [histatin 9] = 0.001 M.

(the ATCUN motif), is the most stable complex in the entire pH range. In histatins 7 and 9, the imidazole nitrogen of His 4 is the anchoring site for Cu(II), showing comparable stability (Fig. 3A).

Quite a surprising issue is observed for zinc(II) complexes (Fig. 3B). Our aim was to observe and explain differences in complex stabilities due to the presence or absence of C-/N-terminal Arg residues – arginines carry a significant positive charge and could theoretically have a stabilizing effect on the complexes by forming hydrogen bonds between the positively charged NH_2 group of the Arg side chain and the backbone carbonyl oxygens[55] or other electrostatic effects and less strong interactions with the solvent molecules that are coordinated.[56]

The results are quite far from what was expected – there are barely any differences that can be commented on. Up to pH 9.3, the almost same thermodynamic stability is related to the same coordination mode $\{2N_{im}, O^-\}$. Above pH 10, the Zn(II)-histatin 9 complex becomes somewhat more stable, with the difference not being significantly higher than the measurement error. The stabilities of Zn(II) complexes of histatin 7, in which the Arg residue is present only at the N-terminus, and histatin 9, without Arg residues at the N- and C-termini, are almost identical. We may conclude that surprisingly, the increase of complex stability by a simple electrostatic interaction is not the case in the studied histatin ligands.

None of the histatins studied in this work showed a tendency to change its secondary structure after binding Cu(II) or Zn(II) ions (as confirmed by near-ultraviolet circular dichroism spectroscopy (data not shown)). Thus, the secondary structure does not affect the antimicrobial activity, which is consistent with the results obtained for the other peptides from the histatin family, especially for the complexes of the N-terminal fragment of histatin 3 (histatin 3-4) and the N-terminal fragment of histatin 5 (histatin 5-8), which, although after binding Zn(II), tend to adopt an α-helical structure, and yet the activity of the complexes is not higher than that of the native peptides.[33,34] Also, Cu(II)/Zn(II) binding does not significantly enhance the antimicrobial activity of the histatins studied in this work and no relationship was observed between the stability of the complexes and their antimicrobial activity – the mechanism of their action is not based on the process of nutritional immunity (AMPs bind metal ions so that microbes cannot get enough metals essential for their life and virulence).

What then influences the antimicrobial activity of histatins and their complexes and the mechanism of their action? Undoubtedly, the pH of the environment has an impact on biological activity. This is related to the cationic nature of histatins – a positively charged peptide interacts more easily with the negatively charged membrane of microorganisms. Previous studies have shown that the anticandidal activity of histatins increases at mildly acidic pH,[22,33] similar to that found in cariogenic plaque, which can reach pH values as low as 5.5. In this sense, the reported MIC values at pH 7.40 should be regarded as conservative estimates of activity under more acidic, clinically relevant conditions.

The effective binding of histatin 1 to the surface of hydroxyapatite is another significant factor that protects it from proteolytic enzyme activity. In addition, specific protease inhibitors present in saliva inhibit protease activity, thereby prolonging the presence and activity of histatin 1 in the oral cavity and indirectly maintaining its functional concentration at the site of action.[57]

The hydrolysis of the genetically encoded histatin 1 and histatin 3 into smaller, often more active fragments, suggests a functional adaptation rather than a simple degradation process. Histatin 1, due to its high affinity for tooth enamel, plays a key role in the formation of the acquired enamel pellicle, where it undergoes controlled proteolysis.[58] This localized hydrolysis may serve as a regulatory mechanism, ensuring that the antimicrobial activity of histatins is maximized precisely where it is needed – at the interface between the enamel and the oral microbiome. The enhanced activity of hydrolysis products highlights the importance of peptide fragmentation as a factor modulating their biological function, which should be considered when designing synthetic analogues or peptide-based therapeutics.

Conclusions

Histatins form thermodynamically stable complexes with Cu(II) and Zn(II). Cu(II) engages ATCUN sites when available, whereas Zn(II) binds *via* –HEXXH– coordination across sequences. Despite robust binding, metallation does not yield a systematic gain in antimicrobial potency: MIC values are modest and largely decoupled from complex stability, indicating that metal coordination is a context-dependent modulator rather than a universal activity switch.

Across the Zn(II) series, coordination involves two His imidazoles and a Glu carboxylate within the –HEXXH– motif, but sequence context governs performance. Histatin 8 shows the expected Cu(II) robustness due to ATCUN chemistry, whereas the Zn(II) complexes of histatin 7 and 9 display near-overlapping thermodynamics over most of the pH range. The strong polarizing character of Zn(II), particularly when an aqua ligand completes a three-nitrogen coordination sphere, likely contributes to these subtle speciation differences without directly boosting antimicrobial potency. Terminal arginine additions do not measurably stabilize Zn(II) binding or enhance killing, underscoring the limits of simple electrostatics.

Metallation does not measurably alter the secondary structure under our conditions, and no clear link emerges between conformation and activity. Together with the weak MIC–stability relationship, this argues against nutritional immunity as the dominant mechanism for these peptides.

Overall, three environmental factors dominate efficacy: localization on the enamel/pellicle (concentrates peptides and limits proteolysis), pH-dependent protonation (helps to interact with pathogen membranes and strengthens surface binding), and metal availability. In this context, proteolysis of histatin 1 or 3 redistributes charge and places active fragments at the enamel–biofilm interface.

Design implications follow directly from this context: aim for pellicle targeting, tune net cationic charge *via* pH or the protonation state rather than only by residue additions, adjust Zn(II)/Cu(II) binding to modulate speciation and conformation as needed but not as a sole lever of potency, and favour compact, optimized fragments that retain enamel affinity.

Author contributions

E. D., A. M-T., L. P-S., K. S., M. B-O., J. W., A. M.-W., and M. R-Ż. conceived and planned the experiments. E. D., A. M.-T. and L. P-S. conducted the experiments. E. D., A. M-T., L. P-S., K. S., M. B-O., A. M.-W., J. W and M. R.-Ż. analysed the results. All authors reviewed the manuscript.

Data availability

The data supporting the article have been included as part of the supplementary information (SI). Supplementary information is available. See DOI: https://doi.org/10.1039/d5dt02485d.

If any additional questions regarding experimental details may arise, the corresponding authors remain at the readers' disposal.

Conflicts of interest

There are no conflicts to declare.

Acknowledgements

Support from the National Science Centre (UMO-2022/47/O/ST4/01865) is gratefully acknowledged.

References

1 E. C. Veerman, P. A. van den Keybus, A. Vissink and A. V. Nieuw Amerongen, *Eur. J. Oral Sci.*, 1996, **104**, 346–352.
2 K. Yamasaki and R. L. Gallo, *Eur. J. Dermatol.*, 2008, **18**, 11–21.
3 S.-U. Gorr, *Periodontology*, 2009, **51**, 152–180.
4 W.-I. Chang, J.-Y. Chang, Y.-Y. Kim, G. Lee and H. S. Kho, *Arch. Oral Biol.*, 2011, **56**, 885–890.
5 S. S. Schwartz, D. I. Hay and S. K. Schluckebier, *Calcif. Tissue Int.*, 1992, **50**, 511–517.
6 F. G. Oppenheim, T. Xu, F. M. McMillian, S. M. Levitz, R. D. Diamond, G. D. Offner and R. F. Troxler, *J. Biol. Chem.*, 1988, **263**, 7472–7477.
7 M. Campese, X. Sun, J. A. Bosch, F. G. Oppenheim and E. J. Helmerhorst, *Arch. Oral Biol.*, 2009, **54**(4), 345–353.
8 M. Castagnola, T. Cabras, G. Denotti, M. B. Fadda, G. Gambarini, A. Lupi, I. Manca, G. Onnis, V. Piras, V. Soro, S. Tambaro and I. Messana, *Biol. Rhythm Res.*, 2002, **33**, 213–222.
9 D. A. Johnson, C. K. Yeh and M. W. Dodds, *Arch. Oral Biol.*, 2000, **45**, 731–740.
10 M. Campese, X. Sun, J. A. Bosch, F. G. Oppenheim and E. J. Helmerhorst, *Arch. Oral Biol.*, 2009, **54**, 345–353.
11 X. Sun, E. Salih, F. G. Oppenheim and E. J. Helmerhorst, *FASEB J.*, 2009, **23**, 2691–2701.
12 I. Messana, T. Cabras, E. Pisano, M. T. Sanna, A. Olianas, B. Manconi and M. Castagnola, *Mol. Cell. Proteomics*, 2008, **7**, 911–926.
13 S. Puri and M. Edgerton, *Eukaryotic Cell*, 2014, **13**(8), 958–964.
14 S. E. Conklin, E. C. Bridgman, Q. Su, P. Riggs-Gelasco, K. L. Haas and K. J. Franz, *Biochemistry*, 2017, **56**(32), 4244–4255.
15 H. Du, S. Puri, A. McCall, H. L. Norris, T. Russo and M. Edgerton, *Front. Cell. Infect. Microbiol.*, 2017, **7**, 41.
16 K. Takano, D. Malamud, A. Bennick, F. G. Oppenheim and A. R. Hand, *Crit. Rev. Oral Biol. Med.*, 1993, **4**, 399–405.
17 M. Ahmad, M. Piludu, F. G. Oppenheim, E. J. Helmerhorst and A. R. Hand, *J. Histochem. Cytochem.*, 2004, **52**, 361–370.
18 D. Shah, M. Ali, Z. Pasha, A. J. Jaboori, S. H. Jassim, S. Jain and V. K. Aakalu, *PLoS One*, 2016, **11**, e0148018.
19 T. Yaguchi and Y. Kawakami, PATENT WO/2012/023588A1, 2012.
20 W. Wongpanuwich, S. Yodsanga, R. Chaisuparat and P. Amornphimoltham, *Anticancer Res.*, 2022, **42**, 2689–2699.
21 P. Jenwanichkul and P. Amornphimoltham, *Exp. Oncol.*, 2024, **46**(2), 101–109.
22 T. Xu, S. M. Levitz, R. D. Diamond and F. G. Oppenheim, *Infect. Immun.*, 1991, **59**(8), 2549–2554.
23 A. Shimotoyodome, H. Kobayashi, I. Tokimitsu, T. Matsukubo and Y. Takaesu, *Caries Res.*, 2006, **40**, 403–411.
24 R. Vitorino, M. J. Lobo, J. R. Duarte, A. J. Ferrer-Correia, P. M. Domingues and F. M. Amado, *Biomed. Chromatogr.*, 2005, **19**, 214–222.
25 X. Sun, X. Huang, X. Tan, Y. Si, X. Wang, F. Chen and S. Zheng, *J. Transl. Med.*, 2016, **14**, 240.
26 J. Driscoll, Y. Zuo, T. Xu, J. R. Choi, R. F. Troxler and F. G. Oppenheim, *J. Dent. Res.*, 1995, **74**, 1837–1844.
27 W. L. Siqueira, H. C. Margolis, E. J. Helmerhorst, F. M. Mendes and F. G. Oppenheim, *J. Dent. Res.*, 2010, **89**, 626–630.
28 H. C. Margolis, S. Y. Kwak and H. Yamazaki, *Front. Physiol.*, 2024, **5**, 339.
29 E. E. McDonald, H. A. Goldberg, N. Tabbara, F. M. Mendes and W. L. Siqueira, *J. Dent. Res.*, 2011, **90**, 268–272.
30 M. J. Oudhoff, J. G. Bolscher, K. Nazmi, H. Kalay, W. Van't Hof, A. V. Amerongen and E. C. Veerman, *FASEB J.*, 2008, **22**, 3805–3812.
31 P. Torres, M. Castro, M. Reyes and V. A. Torres, *Oral Dis.*, 2018, **24**, 1150–1160.
32 I. A. Van Dijk, E. C. I. Veerman, E. A. J. Reits, J. G. M. Bolscher and J. Stap, *Biol. Chem.*, 2018, **399**, 1409–1419.
33 E. Dzień, J. Wątły, A. Kola, A. Mikołajczyk, A. Miller, A. Matera-Witkiewicz, D. Valensin and M. Rowińska-Żyrek, *Dalton Trans.*, 2024, **53**, 7561–7570.
34 E. Dzień, J. Wątły, A. Hecel, A. Mikołajczyk, A. Matera-Witkiewicz, M. Adrover, M. Barceló-Oliver, A. Domínguez-Martín and M. Rowińska-Żyrek, *Dalton Trans.*, 2024, **53**, 19202–19213.
35 L. Sabatini and E. Azen, *Biochem. Biophys. Res. Commun.*, 1989, **160**, 495–502.
36 G. Gran, *Acta Chem. Scand.*, 1950, **4**, 559–577.
37 P. Gans and B. O'Sullivan, *Talanta*, 2000, **51**, 33–37.
38 P. Gans, A. Sabatini and A. Vacca, *Talanta*, 1996, **43**, 1739–1753.
39 L. Petitt, IUPAC Stability Constants Database, Vol. 23, Chemistry International – Newsmagazine for IUPAC, 2001.
40 L. Alderighi, P. Gans, A. Ienco, D. Peters, A. Sabatini and A. Vacca, *Coord. Chem. Rev.*, 1999, **184**, 311–318.
41 International Organization for Standardization, Susceptibility testing of infectious agents and evaluation of performance of antimicrobial susceptibility test devices–Part 1: Broth micro-dilution reference method for testing the *in vitro* activity of antimicrobial agents against rapidly growing aerobic bacteria involved in infectious diseases, 2019.
42 International Organization for Standardization, Clinical laboratory testing and *in vitro* diagnostic test systems–Reference method for testing the *in vitro* activity of antimicrobial agents against yeast fungi involved in infectious diseases, 2012.
43 J. Gabrielson, M. Hart, A. Jarelov, I. Kuhn, D. McKenzie and R. Mollby, *J. Microbiol. Methods*, 2002, **50**, 63–73.
44 F. L. Francisco, A. M. Saviano, T. D. J. A. Pinto and F. R. Lourenço, *J. Microbiol. Methods*, 2014, **103**, 104–111.
45 P. Sabaeifard, A. Abdi-Ali, M. R. Soudi and R. Dinarvand, *J. Microbiol. Methods*, 2014, **105**, 134–140.
46 The European Committee on Antimicrobial Susceptibility Testing, Breakpoint tables for interpretation of MICs and

zone diameters, Version 14.0, 2024, https://www.eucast.org (accessed on 31 March 2025).
47 The European Committee on Antimicrobial Susceptibility Testing, Breakpoint tables for interpretation of MICs for antifungal agents, version 10.0, 2020. https://www.eucast.org/astoffungi/clinicalbreakpointsforantifungals/ (accessed on 31 March 2025).
48 G. Repetto, A. Del Peso and J. L. Zurita, *Nat. Protoc.*, 2008, **3**, 1125–1131.
49 A. Miller, A. Matera-Witkiewicz, A. Mikołajczyk-Tarnawa, A. Kola, M. Wiloch, M. Jonsson-Niedziolka, R. Wieczorek, J. Wątły, D. Valensin and M. Rowińska-Żyrek, *Chem. Sci.*, 2025, **16**, 3447–3458.
50 J. Wątły, K. Szarszoń, A. Mikołajczyk, M. Grelich-Mucha, A. Matera-Witkiewicz, J. Olesiak-Bańska and M. Rowińska-Żyrek, *Inorg. Chem.*, 2023, **62**, 19786–19794.
51 A. Hecel, A. Kola, D. Valensin, H. Kozłowski and M. Rowińska-Żyrek, *Inorg. Chem.*, 2020, **59**, 1947–1958, *Express*.
52 A. Miller, A. Matera-Witkiewicz, A. Mikołajczyk, R. Wieczorek and M. Rowińska-Żyrek, *Inorg. Chem.*, 2021, **60**, 12730–12734.
53 J. Huang, B. J. Jones and R. J. Kazlauskas, *Biochemistry*, 2015, **54**(28), 4330–4341.
54 L. Adibi, P. Yaghmaei, P. Maghami and A. Ebrahim-Habibi, *AMB*, 2024, **14**(1), 69.
55 C. L. Jr Borders, J. A. Broadwater, P. A. Bekeny, J. E. Salmon, A. S. Lee, A. M. Eldridge and V. B. Pett, *Protein Sci.*, 1994, **3**(4), 541–548.
56 S. Leveraro, M. D'Accolti, E. Marzola, E. Caselli, R. Guerrini, M. Rowińska-Żyrek, M. Remelli and D. Bellotti, *J. Inorg. Biochem.*, 2025, **262**, 112761, DOI: 10.1016/j.jinorgbio.2024.112761.
57 T. Baumann, S. H. Niemeyer, M. A. R. Buzalaf and T. S. Carvalho, *Sci. Rep.*, 2023, **13**, 8618.
58 C. F. Richardson, M. Johnsson, P. A. Raj, M. J. Levine and G. H. Nancollas, *Arch Oral Biol.*, 1993, **38**(11), 997–1002.